Chaos in Hamiltonian systems subjected to parameter drift

Cite as: Chaos **29**, 121105 (2019); https://doi.org/10.1063/1.5139717
Submitted: 22 November 2019 . Accepted: 09 December 2019 . Published Online: 27 December 2019

Dániel Jánosi, and Tamás Tél

Chaos in Hamiltonian systems subjected to parameter drift

Cite as: Chaos **29**, 121105 (2019); doi: 10.1063/1.5139717
Submitted: 22 November 2019 · Accepted: 9 December 2019 ·
Published Online: 27 December 2019

Dániel Jánosi[1,a)] and Tamás Tél[1,2,b)]

AFFILIATIONS

[1]Institute for Theoretical Physics, Eötvös Loránd University, Pázmány Péter Sétány 1/A, H-1117 Budapest, Hungary
[2]MTA-ELTE Theoretical Physics Research Group, Pázmány Péter Sétány 1/A, H-1117 Budapest, Hungary

[a)]**Electronic mail:** janosidaniel22@gmail.com
[b)]**Electronic mail:** tel@general.elte.hu

ABSTRACT

Based on the example of a paradigmatic low-dimensional Hamiltonian system subjected to different scenarios of parameter drifts of non-negligible rates, we show that the dynamics of such systems can best be understood by following ensembles of initial conditions corresponding to tori of the initial system. When such ensembles are followed, toruslike objects called snapshot tori are obtained, which change their location and shape. In their center, one finds a time-dependent, snapshot elliptic orbit. After some time, many of the tori break up and spread over large regions of the phase space; however, one may find some smaller tori, which remain as closed curves throughout the whole scenario. We also show that the cause of torus breakup is the collision with a snapshot hyperbolic orbit and the surrounding chaotic sea, which forces the ensemble to adopt chaotic properties. Within this chaotic sea, we demonstrate the existence of a snapshot horseshoe structure and a snapshot saddle. An easily visualizable condition for torus breakup is found in relation to a specific snapshot stable manifold. The average distance of nearby pairs of points initiated on an original torus at first hardly changes in time but crosses over into an exponential growth when the snapshot torus breaks up. This new phase can be characterized by a novel type of a finite-time Lyapunov exponent, which depends both on the torus and on the scenario followed. Tori not broken up are shown to be the analogs of coherent vortices in fluid flows of arbitrary time dependence, and the condition for breakup can also be demonstrated by the so-called polar rotation angle method.

Recently, there has been increasing interest in complex systems that are subjected to arbitrary time-dependent forcing or parameter changes. Within this class, cases with parameter drift are mainly motivated by climate change, as atmospheric carbon dioxide concentration, the driving force of the greenhouse effect, has been observed to increase monotonously for decades. Because dissipative processes are important in the Earth's system dynamics, climate related studies focus on dissipative, non-Hamiltonian cases. The subject of this paper, however, is the problem of low-dimensional Hamiltonian systems with arbitrary time dependence, which has attracted much less attention.

I. INTRODUCTION

A few examples where such systems are of interest should be mentioned here. The question of adiabatic invariants is a central problem of classical mechanics but, with the exception of quasistatically slow cases,[1–4] very little is known about what happens in the case of general time dependence. The emerging field of Lagrangian coherent structures aims at the understanding of advection patterns in flows of arbitrary time dependence.[5] In incompressible cases, the dynamics of passive advection is volume preserving and is thus, in some sense, analogous to Hamiltonian dynamics; a direct application to mechanical problems is, however, still sparse (see, e.g., Refs. 6 and 7). Another field to mention is plasma physics, where, in lowest approximation, charged particles follow the magnetic field lines. A chaotic layer at the border of the plasma is long known to enhance the confinement of particles to the core.[8,9] The efforts to control plasma wall interactions concentrate on manipulating the time-dependent magnetic structure at the plasma edge, the boundary between Kolmogorov-Arnold-Moser (KAM) tori and extended chaos.[10,11] An additional recent direction, where time dependence is important in a Hamiltonian system, is that related to ultracold atoms. Here, a control parameter is swept (and sometimes changed back to its initial value), and one is interested

in qualitative changes found by the end of the scenario.[12,13] These changes are expected to become visible in experiments, too.

The literature on dissipative cases (see, e.g., Ref. 14) concentrates on attractors, phase space objects, to which all trajectories converge. For cases with arbitrary time-dependence, the concept of a snapshot attractor, an attracting object that itself moves in time, was introduced.[15–20] Here, long-term investigation of single trajectories is inappropriate because the system itself changes significantly over a long period of time. A consistent picture of general time-dependent dynamics and its snapshot attractor can only be obtained by launching trajectories from a large number of different initial conditions, i.e., following an initially extended ensemble in the phase space. This way, one obtains (after some transient time, over which the initial conditions become forgotten) the snapshot attractor as the image of the ensemble in a given but changing time instant.[21] This approach has successfully been applied to large-scale climate models (for recent applications, see Refs. 22 and 23) and to turbulence-related experiments.[24]

Although attractors do not exist in Hamiltonian systems (the system does not forget its initial conditions), a lesson of dissipative cases is worth taking according to which single trajectories are not representative; that is, we need to follow trajectory ensembles to statistically characterize the dynamics. It is also worth adopting the view that long-time observations are impossible; therefore, one should concentrate on finite-time behavior.

We show that monitoring an extended ensemble covering initially a large part of the phase space would lead to an unstructured view of the dynamics. A clear characterization is obtained, however, when monitoring special subensembles, corresponding to KAM tori of the initial phase space. As time goes on, these ensembles evolve, their shapes become deformed, and they translate in the phase space. As long as they can be considered to be closed curves not subjected to strong stretching, we call them *snapshot tori* at any instant of time. In their centers, one finds *snapshot elliptic points* (SEPs), moving points with locally elliptic nearby dynamics all the time. Being exposed to parameter drift, at some point, most of the tori start to break up; i.e., they cease to appear as closed curves by experiencing intense stretching.

This transition is due to the fact that the snapshot torus collides with a surrounding chaotic sea. This chaotic sea is also time-dependent, and its extension might increase in time. Within the chaotic sea, one typically finds an orbit with locally hyperbolic nearby dynamics. We call such a point as a *snapshot hyperbolic point* (SHP). When constructing its stable and unstable manifolds, they are found to intersect at a large number of points at any time: a *snapshot horseshoe* or a *snapshot chaotic saddle*[25] is created.

We shall see that torus breakup occurs when a torus collides with a stable manifold of an SHP belonging to a *later* time instant. Examining the average distance of point pairs on the ensemble of an initial torus, we find that it is changing very slowly until the snapshot torus breaks up, but then its growth becomes exponential and the subensemble starts exhibiting chaotic characteristics.

II. THE MODEL

We consider a paradigmatic low-dimensional Hamiltonian example, the periodically forced Duffing oscillator,

$$\ddot{x} = x - x^3 + \varepsilon \cos \omega t, \tag{1}$$

investigated, e.g., in Ref. 6. The time unit is set here by the linear term, and ω represents a dimensionless frequency. We perform a stroboscopic mapping by considering the instants $t = TN$, where $T = 2\pi/\omega$ is the driving period and N is a positive integer. The system possesses a typical divided phase space consisting of a mixture of quasiperiodic tori (with elliptic fixed points at their centers) and chaotic seas (containing hyperbolic fixed points). The overall outlook of the phase portraits largely depends on the driving amplitude ε; as its value rises, the chaotic area grows in size, as Fig. 1 illustrates.

We introduce a parameter drift by adding, for simplicity, a linearly time-dependent term to the initial driving amplitude ε by making the ramp $\varepsilon \to \varepsilon + \alpha t$, where α is the *rate* of the parameter change. We thus obtain the differential equation,

$$\ddot{x} = x - x^3 + (\varepsilon + \alpha t) \cos \omega t, \quad t \geq 0. \tag{2}$$

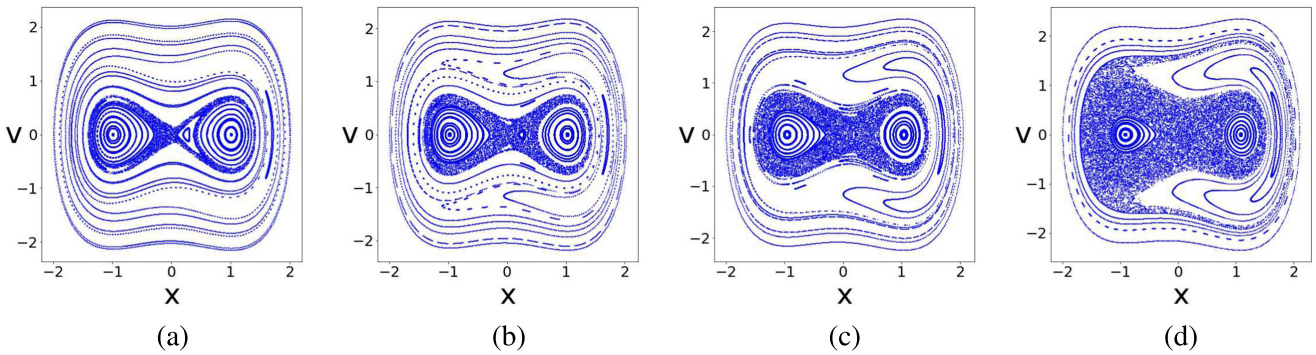

FIG. 1. Phase portraits of the stroboscopically mapped Duffing oscillator (1) for different fixed driving amplitudes $\varepsilon = 0.01, 0.02, 0.04,$ and 0.08 in panels (a), (b), (c), and (d), respectively. Trajectories were launched from 41 initial conditions spreading symmetrically between -2 and $+2$ in x, with $v = \dot{x} = 0$, and were followed in (1) for $N = 1000$ iterations with $\omega = 1$.

This corresponds to the Hamiltonian $H(p,x,t) = p^2/2 - x^2/2 + x^4/4 - x(\varepsilon + \alpha t)\cos\omega t$. The total energy is not constant due to the forcing; instead, in the presence of this ramped scenario, it is monotonically changing on average (increases for $\alpha > 0$). We keep on using the stroboscopic mapping taken at the instances $t = Tn$, where n shall be called the iteration number. We define a *scenario*, starting at time $t = 0$, as the evolution of the driving amplitude set by parameters ε and α, and the number of periods up to which dynamics (2) is followed.

III. THE CHOICE OF ENSEMBLES

When starting with an extended ensemble, as typically done in dissipative cases,[15] one obtains an unstructured pattern, as demonstrated in Fig. 2. Searching for the possible reasons of this lack of structures, one might think that the basic components of the phase space, tori and chaotic seas, can both be imagined to become time-dependent, and the extended ensemble is too crude to distinguish between these components.

Let us, therefore, select a more specific ensemble, concentrated on one of the basic components of the phase space. Being one-dimensional objects and simpler than chaotic seas, let us take the *tori of system* (1), which can be called the *tori of the initial phase space*. The process is as follows. We take a couple of points outside of the chaotic seas of system (1) as initial conditions. Then, we determine the tori belonging to these points using a large number, N, of iterates. Next, we take these tori as initial ensembles and evolve them under (2). As a first trial, let us follow 3 tori, lying in different regions of the original phase space, for a short period of time. As Fig. 3 illustrates, they all remain closed curves by the end of the scenario! We thus see that tori might survive the parameter drift, and it is indeed useful to work with subensembles representing them. These ensembles trace out closed curves, which become stretched and twisted compared to the initial one. Because they change in time, we call them *snapshot tori* (closed curves of the instantaneous phase space) at any instant.

For how long a subensemble represents a slightly deformed curve will depend on both the initial torus and the whole scenario. To illustrate this, we take a set of small initial tori and follow the corresponding ensembles for a longer period of time. Figure 4 illustrates that the outer torus becomes more deformed than the inner ones, and after 7 periods, it develops sharp tongues [panel (c)] and the extension of the set doubles. Up to this instant, all tori appear not to have been subjected to strong stretching. One period later, however, the extension of the outer torus becomes about seven times larger, and the splitting of the curve into a set of points indicates strong stretching. (The splitting is of course the consequence of a finite number of points, N, representing the subensemble, while with a much larger number, a sudden increase in the distance between neighboring points would indicate strong stretching.)

We thus see that after some time, tori start experiencing massive stretching. This process is called the *breaking up* of tori; in Fig. 4(d), the outer torus breaks up at a critical iteration number $n_c = 8$ (a blow-up would show that the inner four ones are still intact at this instant). The starting point of the breaking up depends clearly on the full scenario (ε, α) and the initial torus.

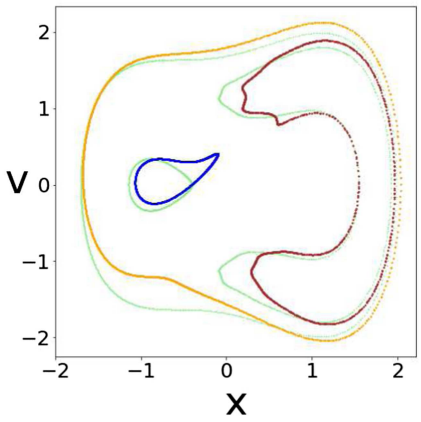

FIG. 3. Three snapshot tori (colored curves) after 2 iterations. First, three initial conditions $x = -1.7, -0.4,$ and 1.55 while $v = 0$ were iterated $N = 1000$ times under (1) with $\varepsilon = 0.1$, $\omega = 1$ forming the light green curves. Then, the points consisting of these tori were taken as initial conditions for (2) and iterated with scenario $\varepsilon = 0.1$, $\alpha = 0.005$ over $n = 2$ periods, which led to the snapshot tori shown here. It is remarkable to see that the tori remained closed (but deformed) curves.

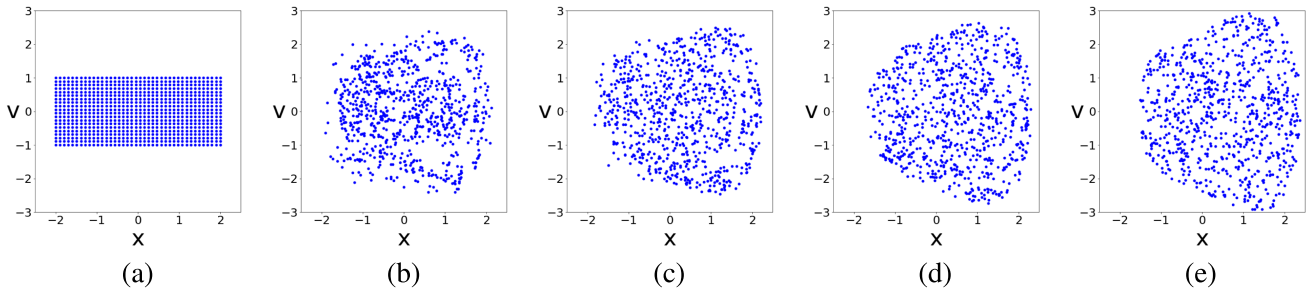

FIG. 2. Evolution of an ensemble of 800 points under (2) followed for 100 iterations of the stroboscopic map in the scenario $\varepsilon = 0.01, \alpha = 0.001$, with $\omega = 1$. The iteration numbers in panels (a)–(e) are $n = 0$, 25, 50, 75, and 100. The ensemble was initially forming the rectangle (a) -2 to $+2$ in x and -1 to $+1$ in v. We clearly see that no structured pattern emerges in this extended ensemble. By the end of the scenario, we have scanned through the stationary cases of all the panels of Fig. 1.

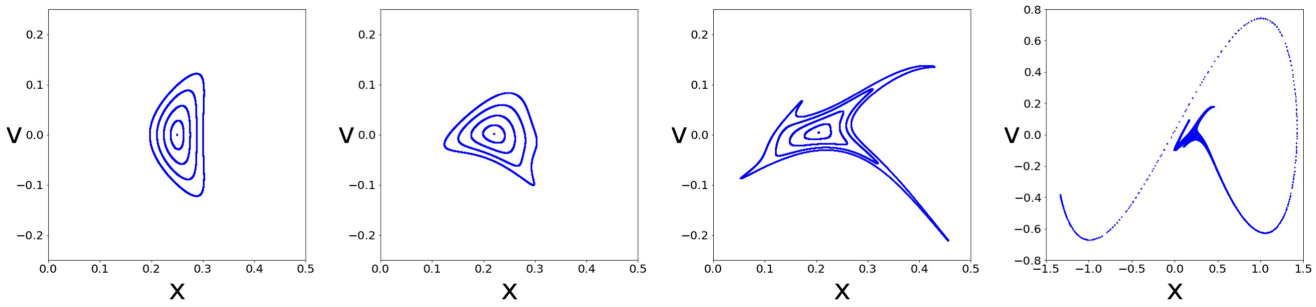

FIG. 4. Evolution of a set of tori captured in the instants $n = 0, 4, 7$, and 8. Five initial conditions, spread evenly between $x = 0.25$ and 0.3 while $v = 0$, were iterated $N = 5000$ times under (1) with $\varepsilon = 0.01$, $\omega = 1$ forming the tori found in picture (a). Then, the points consisting of these tori were taken as initial conditions and iterated under (2) with the rate $\alpha = 0.001$, which led to the sequence of snapshot tori shown here. One can observe the twisting and stretching of the tori in (b) and (c), where the latter can be considered as the last instant before the outermost torus breaks up in (d) (note the different scales of the panels).

IV. SNAPSHOT ELLIPTIC POINTS

At the center of a set of tori of the stationary cases, there is an elliptic fixed point. In our case, however, this point moves together with the set of snapshot tori and is, therefore, called a *snapshot elliptic point (SEP)*. In certain regions, we can obtain analytic expressions for the position of such points. When expanding the equation of motion (2) about the stable locations $x = \pm 1$ of the undriven system, for the deviation δ, one obtains a linear equation subjected to external driving $(\varepsilon + \alpha t)\cos\omega t$. This is an inhomogeneous linear problem, which can be solved by standard methods (for details, see Sec. S1 in the supplementary material).

The homogeneous part of the equation is exactly the same as in the undriven problem and describes a harmonic oscillation with eigenvalues $\lambda_\pm = \pm i\sqrt{2}$. The time-dependent particular solution can, however, be considered as the locus $\delta^*(t)$ of the central oscillatory dynamics. Note that such an elliptic point is not just a point with imaginary local eigenvalues, but a point that *keeps this property* while moving for a long time. For simplicity, we give here the result only for the case $\omega = 1$, which is taken in all examples of the main text. For the x, v coordinates of the SEPs, we obtain for $t \geq 0$,

$$x_E^*(t) = \pm 1 + \delta^*(t) = \pm 1 + (\varepsilon + \alpha t)\cos t + 2\alpha \sin t, \qquad (3)$$

and $v_E^* = \dot{x}_E^*(t)$. Taken at integer multiples n of the period, we find

$$x_{E,n}^* = \pm 1 + \varepsilon + \alpha 2\pi n, \quad v_{E,n}^* = 3\alpha. \qquad (4)$$

On the stroboscopic map, these fixed points move uniformly in the positive x direction, by keeping their velocity coordinates unchanged. In continuous time, the fixed points move along a spiral-like curve. A trajectory and its stroboscopic positions are shown in Fig. S1 of the supplementary material, along with numerically obtained snapshot tori about them.

V. SNAPSHOT HYPERBOLIC POINTS AND THEIR MANIFOLDS

There should also be *snapshot hyperbolic points* (SHPs) in the system. [Note that analogous objects have been considered in the literature (see, e.g., Refs. 26–29), termed as distinguished hyperbolic trajectories, hyperbolic cores, or moving hyperbolic points, but we intend to keep the term snapshot here to emphasize that there is a full set of snapshot objects in systems like ours.] One of the SHPs is inherited from the unstable fixed point $x = 0$ of the undriven case. Its behavior can be understood by considering the linear equation obtained from (2) by neglecting the cubic term in it. This is again an inhomogeneous linear equation (for details, see Sec. S2 in the supplementary material). The homogeneous part is exactly the same as in the undriven problem and describes a hyperbolic structure with eigenvalues $\lambda_\pm = \pm 1$ and eigenvectors pointing along the diagonals at any time. The particular solution can be here, too, considered as the locus $x^*(t)$ of the hyperbolic dynamics. We note again that such a hyperbolic point is more than just a point with positive and negative local eigenvalues, rather a point that *keeps this property* along its trajectory over a long time. Its coordinates in the phase space are given (for $\omega = 1$ again) as

$$x_H^*(t) = -\frac{1}{2}(\varepsilon + \alpha t)\cos t + \frac{\alpha}{2}\sin t, \quad v_H^* = \dot{x}_H^*(t). \qquad (5)$$

On the stroboscopic map, we find

$$x_{H,n}^* = -\frac{\varepsilon}{2} - \alpha\pi n, \quad v_{H,n}^* = 0, \qquad (6)$$

a point that moves uniformly in the negative x direction, with a zero velocity coordinate. In continuous time, the snapshot hyperbolic point also moves along a spiral-like curve as Fig. 5(a) shows in gray. Some stroboscopic locations are marked with crosses, indicating the stable and unstable directions by small arrows.

Pieces of the unstable and stable manifolds can be obtained by iterating small intervals taken along the diagonals of the phase space crossing through $x_{H,0}^*$ forward and backward, respectively, up to n periods. The results obtained from intervals of length $dl = 10^{-3}$ after

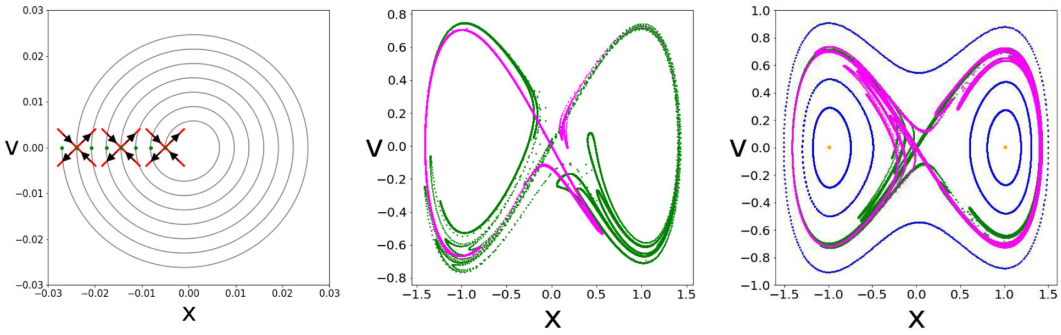

FIG. 5. (a) Time dependence of the analytically obtained SHP of (5) is shown in gray and the stroboscopic values of (6) as green dots for $n = 0, \ldots, 6$ ($\varepsilon = 0.01, \alpha = 0.001$). (b) The pink (green) line represents the stable (unstable) manifold obtained by evolving short intervals about $x^*_{H,0}$ according to (2), plotted at $n = -4(4)$ ($\varepsilon = 0.01$, $\alpha = 0.001$). (c) Stable manifold (pink) initiated at the hyperbolic point $x^*_{H,8}$, and shown at $n = 4$, and unstable manifold (green) initiated at $x^*_{H,0}$, and shown at $n = 4$ as well ($\varepsilon = 0.01, \alpha = 0.0001$). At this instant, a number of intersection points are observed signaling chaotic dynamics. A few surviving tori are also shown in blue on both sides of the manifolds, with the analytically obtained SEPs of (4) for $n = 4$ (orange dots) in their middle.

$n = 4$ periods are shown in Fig. 5(b). On the scale of Fig. 5(a), these manifold pieces would appear to be straight line segments, but on the scale of the whole phase space, they develop folds and tendrils and possess a number of intersection points. This is considered in general to be a sign of chaos.[14] We thus conclude that the snapshot hyperbolic points sit in the middle of chaotic seas, and they are the organizers of chaos in the system.

The intersection points found here do not belong to the same time instant as the stable (unstable) manifolds are plotted at time instants $n = 4$ ($n = -4$). Although the optical impression gained from Fig. 5(b) is convincing, a real horseshoe structure should be unfolded with more care. The intersection points should belong to the same time instant, say, n. To this end, we should consider the stable manifold initiated at $n + n_0$ on a short interval along the subdiagonal about $x^*_{H,n+n_0}$ with a possibly large n_0 and subject it to the backward iteration of length n_0. Analogously, the unstable manifold should be initiated at time $n - n_0$ on a short interval along the diagonal about $x^*_{H,n-n_0}$ and be subjected to the forward iteration of length n_0. By overlaying these manifolds, a *snapshot horseshoe structure* shows up belonging to the time instant n. (The construction of snapshot horseshoes and manifolds of dissipative systems was described in Refs. 25, 30, and 31.)

For illustrative purposes, in our Hamiltonian problem, we take $n = n_0 = 4$ and construct an approximant of the horseshoe for $n = 4$ as Fig. 5(c) illustrates. The character of the figure is not much different from that of Fig. 5(b), but the set of intersection points here can be considered as an approximant of a chaotic saddle,[25] known to be the skeleton of chaos in any case. Thus, we can safely say that there is a chaotic sea about the SHP investigated, i.e., close to the origin of the phase space.

VI. A GEOMETRICAL CONDITION FOR TORUS BREAKUP

In view of the observation that there is chaos, and hence strong stretching about the snapshot hyperbolic point close to the origin $(x, v = 0)$, we can say that the breakup of a torus starts if a point of it comes close to this point. To check if this occurs on the stroboscopic map at time n_c, two curves should be compared. One is the stable manifold of the SHP belonging to time instant n_c obtained by iterating a short segment *backward* exactly n_c times. The other one is a torus in the stationary system of (1) (corresponding to $n = 0$). We might think that these two sets must not intersect, but this is only true in autonomous systems. If an intersection occurs, then one point of the torus is simultaneously on the stable manifold that will transport points to the hyperbolic point by time n_c. The condition for a torus to break up at time n_c is thus that the *initial torus intersects the stable manifold of the SHP belonging to time instant* n_c, obtained by iterating a short interval about it backward n_c times. Since one obtains finite-time manifolds this way, the shape of the manifold depends somewhat on the length dl of the short segment which the iteration starts with. We choose here dl to be comparable with the size of the chaotic sea about the SHP, well approximated by the width of the region foliated by the stable manifold about the origin.

To illustrate this, Fig. 6(a) shows a set of initial tori ($t = n = 0$) among which the red one almost crosses the pink manifold, while in Fig. 6(b), the intersection does occur. Here, the pink curve is the stable manifold of $x^*_{H,5}$ obtained by iterating a short segment about it $n = 5$ times backward. Figures 6(c) and 6(d) show the shape of the red torus after $n = 4$ and $n = 5$ iterations, respectively, of (2). The breakup thus occurs at $n_c = 5$ since points of the torus have reached the vicinity of the origin where a chaotic sea is situated, illustrating that the geometric condition predicts the breakup very well.

The properties found here are rather general. This is illustrated in Sec. S3 of the supplementary material with another case, that of the outermost torus of the set of tori considered in Fig. 6, which is of course found to break up earlier than the red torus here.

It is worth mentioning that there is an extended literature on coherent vortices or elliptic Lagrangian coherent structures in flows of arbitrary time dependence; see, e.g., Refs. 5 and 32–36. In two-dimensional incompressible flows, the passive advection

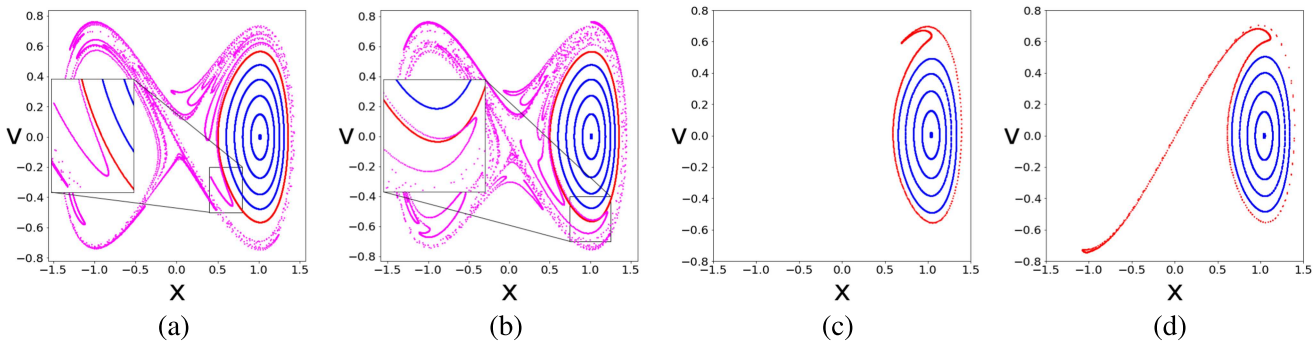

FIG. 6. (a) The stable manifold (pink curve) obtained with $dl = 0.1$ of the SHP $x^*_{H,4}$ plotted at time zero along with the stationary tori generated from initial conditions $x = 0.5$ (red) and $0.6, \ldots, 1$ (blue), $v = 0$. (b) The same set of tori plotted with the stable manifold of $x^*_{H,5}$ viewed at $n = 0$. The insets show the (lack of) intersection between the pink and the red curve in (a) and (b). The points where the two ensembles meet should end up near the SHP $x^*_{H,5}$ when iterated forward 5 times. (c) The red snapshot torus at $n = 4$ and (d) at $n = 5$. As we can see, the breakup of this torus occurs at $n_c = 5$, which is exactly what the geometric condition predicts.

dynamics can be described by means of a time-dependent Hamiltonian (the stream function). Long-lived vortices of such cases correspond to tori, which do not break up. The outermost torus out of a set of concentric tori corresponds to the edge of a vortex living up to n periods at least. Several criteria have been developed to identify coherent fluid vortices (see, e.g., Ref. 5), out of which the so-called polar rotation angle (PRA) method is particularly well suited for an application to any low-dimensional Hamiltonian system.

VII. A MATERIAL ROTATION BASED CONDITION FOR TORUS BREAKUP: THE PRA METHOD

The polar rotation angle (PRA) method, developed by Farazmand and Haller in Ref. 7, aims to characterize systems driven by forcing of arbitrary time dependence in which polar rotation can be described with one angle, the PRA, which is calculated using the singular values and vectors of the flow gradient. With this method, one is able to investigate the phase space structure at the end of a time interval of interest $[0, t]$. The authors show that elliptic coherent structures are characterized by closed *smooth* level curves of the PRA field on the plane of initial conditions. Extrema of the PRA field correspond to centers of coherent regions, SEPs in our terminology. Because of this, we can identify a condition for the breakup of tori in the PRA framework as well, with the following process. By using the freely accessible LCStool MATLAB package[37,38] to generate the PRA field, we iterate system (2) from 0 to t, and additionally, we determine the level curves of this angle. Next, we display our initial torus together with the level curves. If our initial torus lies in a region encircled by smooth level curves means that it would not have been broken up until that instant. This means that if we simulate until $t = 2\pi n_c$, we should see that for times $n < n_c$, our initial torus is among the coherent structures identified by the PRA, while for $n \geq n_c$, the initial torus is partly or entirely surrounded by non-smooth level lines. The result of this comparison can be seen in Sec. S4 of the supplementary material and shows good agreement with the results based on the geometric condition.

VIII. DYNAMICAL INSTABILITY

The dynamical instability of chaotic systems is typically characterized by the average growth rate of distances between pairs of points.[14] One calculates the slope of the quantity $\rho = \ln r(t)$, where $r(t)$ is the distance between a pair of points after time t lying initially very close to each other. The slope of this quantity averaged over several pairs is the Lyapunov exponent of the system.[14]

When generalizing this quantity for a subensemble of a torus, one evaluates the quantity,

$$\rho = \langle \ln r(t) \rangle, \tag{7}$$

where $r(t)$ is the distance of a pair of points at t, which were close to each other *on* the torus at $t = 0$ and the bracket denotes the average *taken over this subensemble*. We expect that there is hardly any change in time before the snapshot torus breaks up. There is no sensitive dependence on initial conditions (supporting the use of the term torus for this object), which can thus be considered as a generalization of quasiperiodic motion in the sense of ensembles. After the breakup, however, an exponential growth is expected to occur expressing the fact that the ensemble is subjected to strong stretching by entering into a chaotic regime. The first curve of Fig. 7(a) illustrates this for a torus for which the exponential growth starts at $n = 31$. Panel (b) confirms that the time instant $n = 30$ is just before breakup, while on panel (c), we can see that $n = n_c = 31$ is indeed a breakup instant. The slope of the exponential growth can be considered as a new type of the finite-time Lyapunov exponent (λ) characterizing the fate of the torus after breakup. The second curve of Fig. 7(a) shows $\rho(t)$ for another, smaller torus, which breaks up much later, at $n_c = 60$, with the Lyapunov exponent being also different.

Having shown in Sec. VI that the breakup of the tori depends on the whole investigated scenario, and together with the fact that the broken-up torus exhibits chaotic characteristics (since it can be described with a new type of the Lyapunov exponents), for each broken-up torus, the whole process can thus be called a scenario-induced transition to chaos.

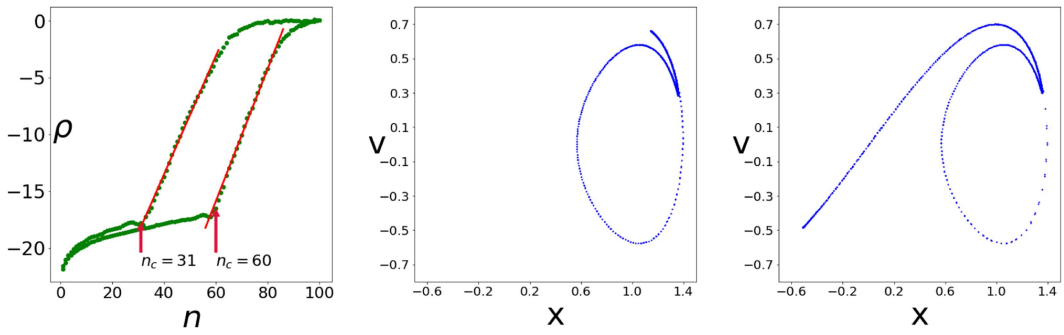

FIG. 7. (a) Quantity $\rho(t)$ of (7) corresponding to two tori, followed for 100 iterations ($\varepsilon = 0.01, \alpha = 0.0001$). Initially, the value does not change much, but at one point, the growth becomes exponential, becoming linear on the logarithmic scale used here. The crossover point is where the breakup happens; for the first curve, it is at $n_c = 31$, as illustrated by panels (b) and (c). For the other curve, $n_c = 60$. The slopes of the fitted linear curves give us the Lyapunov value $\lambda = 0.52 \pm 0.004$ and $\lambda = 0.58 \pm 0.006$. The flat part at the end of the scenario indicates that by that time, pairs of points have reached their maximal distance and extend over the whole phase space.

IX. DISCUSSION AND SUMMARY

The plethora of phenomena related to Hamiltonian systems subjected to parameter drift is rather broad. First, one can also follow the fate of snapshot chaotic seas or, if they are plotted together with sets of snapshot tori, a snapshot phase portrait. We mention here briefly a few such examples. The phase space of the stationary problem (seen in Fig. 1) suggests that the importance of chaos decreases with decreasing driving amplitudes, while the region filled with tori expands. It is, therefore, surprising that in scenarios taken with negative rates, torus breakup also takes place, and the size of the chaotic region in the end state is larger than in the stationary case belonging to this driving amplitude (see Sec. S5 in the supplementary material). Another interesting class of cases is provided by scenarios containing an increasing and decreasing ramp leading to full return. Section S6 in the supplementary material shows that a hysteresis takes place, and the end state deviates from the initial state.

In summary, the investigation of our paradigmatic low-dimensional model illustrates that a divided phase space structure also characterizes Hamiltonian systems driven by forces of arbitrary time-dependence. This structure, however, becomes best visible in a well chosen ensemble view, when subensembles localized on tori are followed in time. The resulting snapshot tori might keep their smooth closed curve structure up to some time. However, when penetrating into a chaotic sea, they break up by becoming suddenly strongly stretched. Their centers are marked by snapshot elliptic points, and the key features inside chaotic seas are snapshot hyperbolic points. An exact expression for their instantaneous position is unlikely to be found in general, but it is important to know that they exist and keep their local stability structure over long stretches of time with not necessarily constant eigenvalues, as in our simple case. The temporal movement of such hyperbolic points shows that they are not periodic, and no periodic orbit exists. Therefore, it is *impossible to carry out periodic orbit expansion*, a central tool of traditional chaos theory.[14,39] The topological complexity of chaos can nevertheless be demonstrated by constructing a snapshot horseshoe in which the generalization of homoclinic orbits appears as intersection points of the stable and unstable manifolds of a moving snapshot hyperbolic point belonging to a given time instant (or practically equivalently, a snapshot chaotic saddle). More generally speaking, we have shown that in the presence of parameter drift, one can construct the snapshot counterpart of any important concept and structure of Hamiltonian dynamical systems theory.

SUPPLEMENTARY MATERIAL

See the supplementary material for analytical calculations of SEPs and SHPs, an additional example for the validity of the geometrical condition, the visualization of the PRA results and their relation to torus breakup, and for two additional types of scenarios: one with decreasing driving amplitude and one resulting in a hysteresis.

ACKNOWLEDGMENTS

We would like to thank G. Györgyi, G. Haller, and C. Jung for the beneficial discussions and comments as well as B. Kaszás and Z. Kaufmann for their help with numerical issues and for useful comments. This work was supported by the Hungarian NKFIH Office under Grant No. K-125171.

REFERENCES

[1] E. Ott, Phys. Rev. Lett. **42**, 1628 (1979).
[2] R. Brown, E. Ott, and C. Grebogi, Phys. Rev. Lett. **59**, 1173 (1987).
[3] R. Brown, E. Ott, and C. Grebogi, J. Stat. Phys. **49**, 511 (1987).
[4] M. Wilkinson, J. Phys. A **21**, 4021 (1988).
[5] G. Haller, Annu. Rev. Fluid Mech. **47**, 137 (2015).
[6] A. Hadjighasem, M. Farazmand, and G. Haller, Nonlinear Dyn. **73**, 689 (2013).
[7] M. Farazmand and G. Haller, Physica D **315**, 1 (2016).
[8] J. S. E. Portela, I. L. Caldas, R. L. Viana, and M. A. F. Sanjuán, Int. J. Bifurcat. Chaos **17**, 4067 (2007).
[9] J. S. E. Portela, I. L. Caldas, and R. L. Viana, Eur. Phys. J. Spec. Top. **165**, 195 (2008).
[10] A. C. Fraile, Jr., M. Roberto, I. L. Caldas, and C. G. L. Martins, IEEE Trans. Plasma Sci. **45**, 2906–2912 (2017).
[11] D. de O. Berto, L. F. Ziebell, and P. R. da S. Rosa, Plasma Phys. Control. Fusion **61**, 065021 (2019).
[12] R. Bürkle, A. Vardi, D. Cohen, and J. R. Anglin, Phys. Rev. A **99**, 063617 (2019).

[13]R. Bürkle, A. Vardi, D. Cohen, and J. R. Anglin, Phys. Rev. Lett. **123**, 114101 (2019).
[14]E. Ott, *Chaos in Dynamical Systems* (Cambridge University Press, Cambridge, 1993).
[15]F. J. Romeiras, C. Grebogi, and E. Ott, Phys. Rev. **A41**, 784 (1990).
[16]Y.-C. Lai, Phys. Rev. E **60**, 1558 (1999).
[17]R. Serquina, Y.-C. Lai, and Q. Chen, Phys. Rev. E **77**, 026208 (2008).
[18]M. Ghil, M. D. Chekroun, and E. Simonnet, Physica D **237**, 2111 (2008).
[19]C. Kuehn, *Multiple Time Scale Dynamics* (Springer, New York, 2015).
[20]M. Ghil, "A mathematical theory of climate sensitivity or, how to deal with both anthropogenic forcing and natural variability," in *Climate Change: Multidecadal and Beyond*, edited by C. P. Chang, M. Ghil, M. Latif, and J. M. Wallace (World Scientific Publishing Co./Imperial College Press, 2013).
[21]G. Drótos, T. Bódai, and T. Tél, J. Clim. **28**, 3275 (2015).
[22]T. Haszpra and M. Herein, Sci. Rep. **9**, 3896 (2019).
[23]B. Kaszás, T. Haszpra, and M. Herein, Chaos **29**, 113102 (2019).
[24]M. Vincze, I. Dan Borcia, and U. Harlander, Sci. Rep. **7**, 254 (2017).
[25]Y.-C. Lai and T. Tél, *Transient Chaos* (Springer, New York, 2011).
[26]K. Ide, D. Small, and S. Wiggins, Nonlinear Process. Geophys. **9**, 237 (2002).
[27]S. Wiggins, *Introduction to Applied Nonlinear Dynamical Systems and Chaos*, 2nd ed. (Springer, Berlin, 2003).
[28]M. Mathur, G. Haller, T. Peacock, J. E. Ruppert-Felsot, and H. L. Swinney, Phys. Rev. Lett. **98**, 144502 (2007).
[29]G. Froyland, Physica D **250**, 1 (2013).
[30]B. Kaszás, U. Feudel, and T. Tél, Phys. Rev. E **94**, 062221 (2016).
[31]B. Kaszás, U. Feudel, and T. Tél, Chaos **28**, 033612 (2018).
[32]G. Haller and F. J. Beron-Vera, J. Fluid Mech. **731**, R4 (2013).
[33]G. Haller, A. Hadjighasem, M. Farazmand, and F. Huhn, J. Fluid Mech. **795**, 136 (2016).
[34]G. Froyland and O. Junge, SIAM J. Appl. Dyn. Syst. **17**, 1891 (2018).
[35]A. G. Ramos *et al.*, Sci. Rep. **8**, 4575 (2018).
[36]G. Froyland, C. P. Rock, and K. Sakellariou, Commun. Nonlinear Sci. Numer. Simul. **77**, 8 (2019).
[37]See https://github.com/LCSETH/LCStool, as a manual, see Ref. 38.
[38]K. Onu, F. Huhn, and G. Haller, J. Comput. Sci. **7**, 26 (2015).
[39]P. Cvitanovic, R. Artuso, R. Mainieri, G. Tanner, and G. Vattay, *Chaos: Classical and Quantum*, edition16.4.2 (ebook, 2019), see chaosbook.org.